45th AIAA Plasmadynamics and Lasers Conference AIAA-2014-2493
16-20 June 2014, Atlanta, GA

Shack-Hartmann Wavefront Measurements of Supersonic Turbulent Boundary Layers in the TGF

Adam E. Smith[1], Stanislav Gordeyev [2]
University of Notre Dame, Notre Dame, Indiana, 46556

Hamza Ahmed[3], Anwar Ahmed[4]
Auburn University, Auburn, AL 36849

Donald J. Wittich III[5] and Michael Paul[6]
Air Force Research Laboratory, Directed Energy Directorate, Kirtland AFB, NM 87117

Aero-optical environment of the supersonic flow in Trisonic Gasdynamic Facility (TGF) wind tunnel at Wright-Patterson AFB was experimentally measured using a high-speed wavefront sensor. Temporally- and spatially-resolved wavefronts were collected at a range of Mach numbers between 1.5 and 3.0 and the range of Reynolds numbers between 1 and 4 million per foot. Several data reduction techniques, including multi-point spectral cross-correlation method, were introduced to analyze results and important statistical information about the turbulent boundary layer was extracted and discussed. A novel method was presented for using the frozen flow assumption to recover time-resolved wavefront measurements from spatially resolved 2-D wavefronts that are under-sampled in time. The criteria for using this technique were discussed in detail.

I. Introduction

IN the region immediately around an aerodynamic vehicle, the presence of turbulent density fluctuations can alter the local speed of light passing into and/or out of the aircraft through the turbulent region. This physical phenomenon, known as the aero-optic problem, is at its root the result of the relationship between index-of-refraction, n, and density in air, ρ, via the Gladstone-Dale constant, K_{GD} (which is approximately 2.27×10^{-4} m^3/kg in air for visible wavelengths of light),

$$n(\vec{x},t)-1=K_{GD}\rho(\vec{x},t). \tag{1}$$

Light passing through regions of unsteady turbulent aerodynamic flow is unsteadily distorted by the spatially- and temporally-fluctuating density fields present along the optical path length. This might pose a significant problem for the performance of airborne optical system, whether they are directed energy, imaging, or free-space communications applications, as small disturbances to optical wavefronts in the near-field can result in significant reductions in time-average and instantaneous on-target intensity at points very far away from the aircraft [1,2].

As planar wavefronts propagate through these unsteady density distributions, the effect of turbulent density fluctuations on the propagation of light can be quantified by defining the Optical Path Length (OPL) as the integral of the index-of-refraction of a medium along the physical length traversed by a ray of light. Since index-of-refraction and density are related via Equation (1), OPL can be expressed as

$$\mathrm{OPL}(x,y,t)=\int_a^b n(x,y,z,t)dz=\int_a^b\left[K_{GD}\rho(x,y,z,t)+1\right]dz. \tag{2}$$

---

[1]Graduate Student, Department of Mechanical and Aerospace Engineering, Hessert Laboratory for Aerospace Research, Notre Dame, IN 46556, Student Member.
[2]Research Associate Professor, Department of Mechanical and Aerospace Engineering, Hessert Laboratory for Aerospace Research, Notre Dame, IN 46556, AIAA Associate Fellow.
[3]Graduate Student, Samuel Ginn College of Engineering, Department of Aerospace Engineering, 211 Davis Hall, Auburn, AL, 36849, Student Member.
[4]Associate Professor, Samuel Ginn College of Engineering, Department of Aerospace Engineering, 211 Aerospace Engineering Bldg., Auburn, AL, 36849, AIAA Associate Fellow.
[5]Aerospace Engineer, Laser Division, 3550 Aberdeen Ave SE, AIAA Member
[6]Aerospace Engineer, Laser Division, 3550 Aberdeen Ave SE, AIAA Member

where z is the direction of beam propagation. The resulting deviation from the average OPL can then be expressed as the Optical Path Difference (OPD),

$$\mathrm{OPD}(\bar{x},t) = \mathrm{OPL}(\bar{x},t) - \overline{\mathrm{OPL}(\bar{x},t)}, \tag{3}$$

where the overbar denotes spatial averaging. It can be shown that OPD is in fact the conjugate of the zero-mean wavefront, $W(\bar{x},t) = -\mathrm{OPD}(\bar{x},t)$.

One of the important fundamental flows responsible for aero-optical aberrations is a turbulent boundary layer [2]. While the turbulence levels inside turbulent boundary levels are smaller than turbulence intensity downstream of turrets, boundary layers, especially at transonic and supersonic speeds, might still cause significant aero-optical distortions causing efficiency degradation in directed energy systems [2,3,4] or disrupting free-space high-bandwidth airborne communication systems [5]. In addition, studying time-resolved aero-optical distortions provides valuable information into the dynamics of large-scale structures of the turbulent boundary layer [3].

While aero-optics of subsonic boundary layers has been extensively studied in recent years [2, 3 and references therein], experimental measurements [4, 6] and numerical simulations [7,8,9] in supersonic boundary layers are very limited and many important questions about the details of underlying aero-optical structure, its dynamics still remain unanswered. Several theoretical models were proposed [6, 4] to predict levels of aero-optical distortions caused by supersonic boundary levels at different Mach and Reynolds numbers, but the additional experimental data are needed to fully verify them.

Extensive experimental measurements of the supersonic boundary layer on walls of the test section in Trisonic Gasdynamics Facility (TGF) were performed in August of 2013 for a range of subsonic and supersonic freestream speeds, Reynolds numbers and boundary layer thicknesses [10]. Two different wavefront sensors were used to collect time-resolved wavefront data, a Malley Probe and a high-speed Shack-Hartmann wavefront sensor. An analysis of the overall aberration levels and an assessment of the Malley Probe data are provided in a companion paper [10] while this paper will focus on the analysis of the Shack-Hartmann Sensor data, which provided 2-D, time-resolved wavefronts.

II. Experimental Setup

The presented experiments were conducted in the Trisonic Gasdynamics Facility (TGF) wind tunnel at Wright-Patterson AFB. The TGF, shown in Figure 1, is a closed circuit, variable density, continuous flow wind tunnel with a cross-section of 61 cm × 61 cm in the tunnel test section [12]. The TGF is able to operate at a range of Mach numbers from 0.23 to 3.0, with several interchangeable nozzle blocks are used to operate at discrete supersonic freestream velocities [13]. Two 71 cm diameter optical quality windows are mounted on the test section sidewalls to allow for Schlieren imaging, PIV, and other optical fluid diagnostic techniques including aero-optic wavefront sensors [12].

Aero-optic characterization of the turbulent boundary layer in the TGF wind tunnel was performed with both the Malley probe 1-D and high-speed Shack-Hartmann 2-D wavefront sensors. Measurements were obtained at Mach numbers 1.5, 1.9, 2.3, and 3.0 for different locations and Reynolds numbers; see Table 1 for a complete description of all cases obtained at the window center location. In addition to wavefront measurements, the time-average sidewall turbulent boundary layer profiles were measured using a total pressure rake as part of this experiment. The estimation of boundary layer thickness from the rake measurements, including interpolation to the test conditions of the optical experiments, is presented in [10].

Spatially- and temporally-resolved two-dimensional wavefront measurements were obtained using the Shack-Hartmann wavefront sensor configuration shown schematically in Figure 2. This arrangement uses a double-pass, double boundary layer (DBL) technique to obtain aero-optic wavefront measurements of the TGF boundary layer in an identical manner to what is done with the Malley probe. Assuming the boundary layers on opposite walls are statistically independent and symmetric, it has been shown that a correction can be applied to the double-pass, DBL wavefront measurements in order to match levels expected from wavefront propagation through a single boundary layer (SBL) [14].

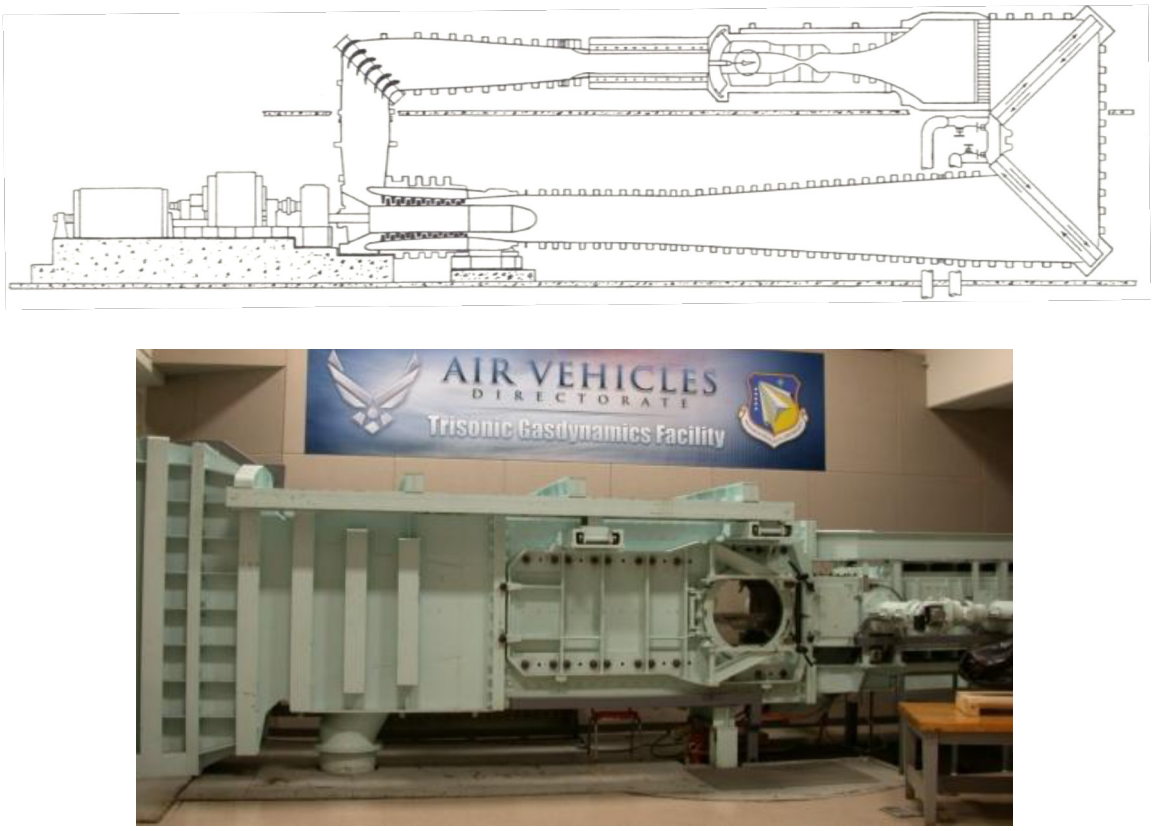

Figure 1. Trisonic Gasdynamics Facility at Wright Patterson AFB, schematic (top) and the test section (bottom).

Mach Number	Reynolds Number [1/ft]				
	1×10^6	2×10^6	3×10^6	4×10^6	4.8×10^6
1.5	◆	◆	❖		
1.9	◆	◆	◆	⊙	
2.3	◆	❖	❖	❖	❖
3.0	◆	◆	◆	❖	

Table 1. Shack-Hartmann wavefront measurements obtained at the window center location with frame rates of ◆ 25 kHz only, ⊙397 kHz only, and ❖ both 25 kHz and 397 kHz.

One set of Shack-Hartmann wavefront measurements was acquired for a circular beam of diameter Ap = 30 mm, with a spatial resolution of 30×30 subapertures using a relatively low sampling rate of 25 kHz and an exposure time of 1 μs for each frame of data. The duration of each sample in time was 0.85 sec. Wavefronts were also obtained for a smaller-spatial resolution of 8×3 subapertures, with 8 subapertures in the streamwise direction, corresponding to a rectangular aperture 8 mm x 3 mm at a higher frame rate of 397 kHz for 1.72 sec, with the same frame exposure time. Both sets of wavefront measurements obtained with the Shack-Hartmann wavefront sensor were reduced using in-house wavefront processing software and time-resolved deflection angles $\theta_x(t)$ and $\theta_y(t)$ and temporally-spatially-resolved, tip-tilt/piston removed $OPD(x,y,t)$ were calculated.

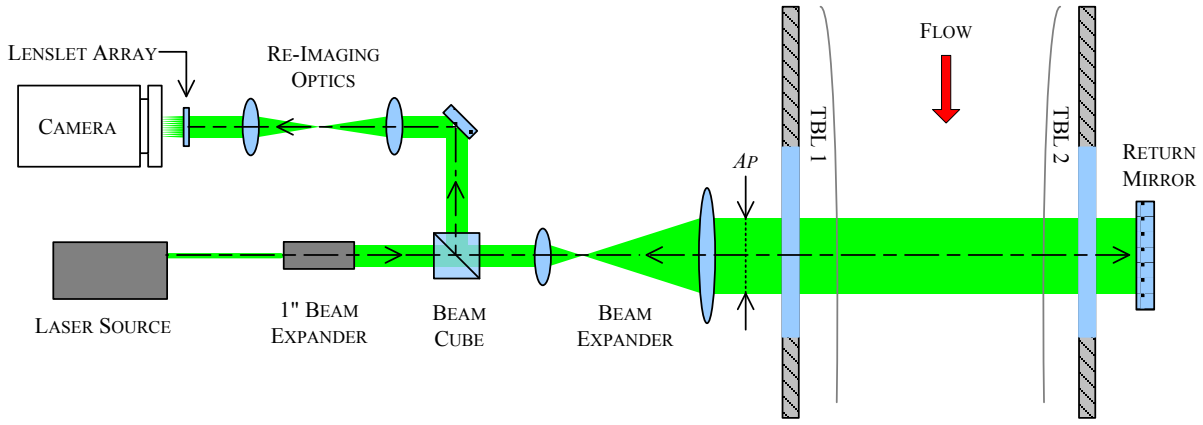

Figure 2. Schematic of Shack-Hartmann 2-D wavefront sensor used to characterize the TGF boundary layer.

The first set of wavefront has wavefronts which are well-resolved in space with 30x30 subapertures, but, as it will be shown later in this paper, are not properly-resolved in time. The second set of wavefronts has sufficient, high-bandwidth, temporal resolution, but clearly provides limited, 8x3 subapertures, spatial resolution. In the following section, both sets of data are analyzed in order to extract aero-optical statistics of the turbulent boundary layer at different Mach and Reynolds numbers.

III. Results

A. Low-Bandwidth, High Spatial Resolution WFS Data

While undersampled wavefront data do not have detailed temporal information about aero-optical structures, they still provide good spatially-resolved wavefronts and overall levels of aero-optical distortions still can be extracted from the data. The aperture function, which accounts for reduction in levels of aero-optical distortions due to finite apertures for subsonic boundary layers was presented in [4] and it was shown that the aperture function is essentially unchanged for the supersonic boundary layer [3]. Thus, using the subsonic boundary-layer aperture function, overall levels of aero-optical distortions can be extracted from collected finite-aperture wavefronts. Results in dimensional form, re-scaled for the single boundary layer, for all measured Mach and Reynolds numbers is presented in Figure 3, left. Overall levels of OPDrms for all tested conditions are fairly small, less than 0.05 microns. As expected, OPDrms generally increases with Reynolds number, as Reynolds number was changed by varying the freestream pressure and thus, the freestream density and OPDrms is proportional to the freestream density.

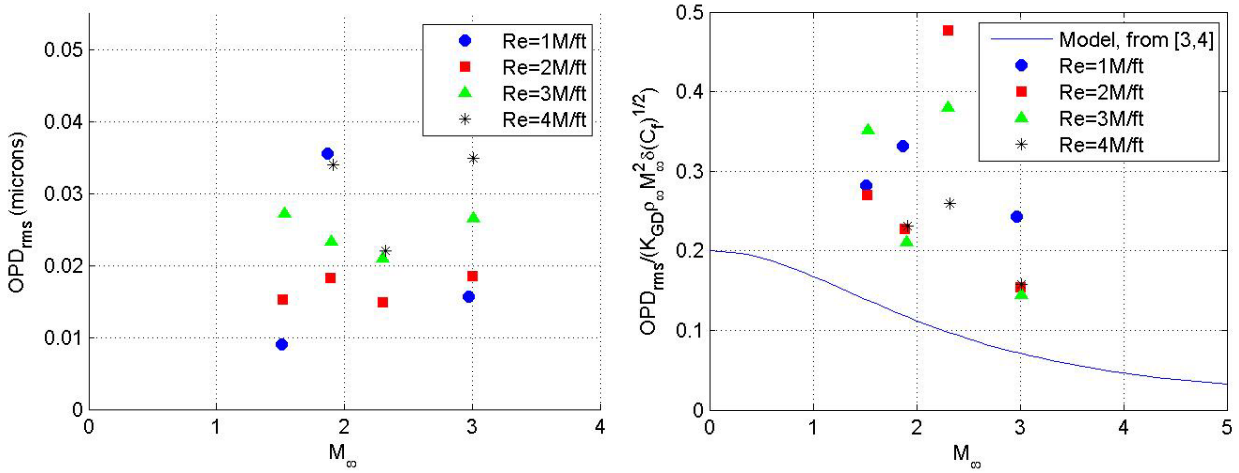

Figure 3. Left: OPD_{rms} for a single boundary layer calculated from high-spatial resolution WFS data. Right: Normalized values of OPD_{rms} calculated from high-spatial resolution WFS data, compared with the theoretical prediction [3,4].

In [3,4] the model for aero-optical distortions for canonical boundary layers was derived, $OPD_{rms} = K_{GD}\rho_\infty M_\infty^2 \delta\sqrt{C_f}F(M_\infty)$. From here it follows that the normalized value of OPDrms, $OPD_{rms}/(K_{GD}\rho_\infty M_\infty^2 \delta\sqrt{C_f})$ is a function of Mach number only, $F(M_\infty)$. Normalized levels of aero-optical distortions, compensated for aperture effects, are shown in Figure 3, right, along with the theoretical prediction from [3,4] and other experimental data [3,4]. Normalized aero-optical levels of the single boundary layer in TGF facility were found to be a factor of two-three times larger than for canonical boundary layers. Analysis of the boundary layer profiles collected in TGF using the curved boundary layer rake [15] had shown that the boundary layer does not have a canonical profile and it is possible that the boundary layer was tripped somewhere upstream of the nozzle. More discussion on the possible reasons of higher-then-canonical levels of aero-optical distortions in TGF will be given in Conclusions section.

B. High-Bandwidth, Low Spatial Resolution WFS Data

The aperture of the laser beam was 30 mm, giving the aperture-to-thickness ratio, Ap/δ, to be between 1.5 and 2.5, as the boundary layer thickness was different for different Mach and Reynolds numbers [10]. In [3,16] it was shown that for relatively small values of Ap/δ, spatial wavefront spectra are corrupted by aperture effects. Due to the mostly convecting nature of the boundary layer wavefronts, it is possible to recover the spatial wavefront spectrum from the temporal deflection angle spectra, using the frozen-field assumption, $x = U_C t$, or, in the spectral domain, $k_x = 2\pi f/U_C$ [16]. The sampling frequency for the high-spatial resolution wavefront data was only 25 kHz, which is insufficient to properly resolve the temporal spectrum due to aliasing issues, although by combining spatial and temporal information it is still possible to recover most of the essential statistics of the boundary layer, see subsection C for details.

High-speed WF data for 8×3 subapertures span only 8 mm in the streamwise direction, so they do not provide detailed spatially-resolved wavefronts. Instead, time series of local deflection angles, sampled at the high framing rate of 397 kHz, can be analyzed and, using the frozen flow assumption, can be converted into the spatially-resolved WF spectra.

Locally, deflection angles, θ, can be assumed to be a combination of a stationary, θ_S, (for instance, mechanical jitter) and traveling, θ_T, (aero-optical structure) modes,

$$\hat{\theta}(x,f) = FT\{\theta(x,t)\} = \hat{\theta}_S(f) + \hat{\theta}_T(f)\exp\left(2\pi i f(t - x/U_C)\right). \quad (4)$$

Assuming that the stationary and the traveling components are statistically-independent, the cross-spectral correlation, S, can be computed between deflection angles for different separations,

$$S(\Delta x; f) = \left\langle \hat{\theta}(x,f)\hat{\theta}^*(x+\Delta x, f)\right\rangle = \left|\hat{\theta}_S(f)\right|^2 + \left|\hat{\theta}_T(f)\right|^2 \exp\left(2\pi i f \Delta x/U_C\right). \quad (5)$$

If the cross-correlation function is known for more than two different separations, the above equation is over-determined, and the convective speeds and stationary and traveling spectra can be found using the least-squared estimation.

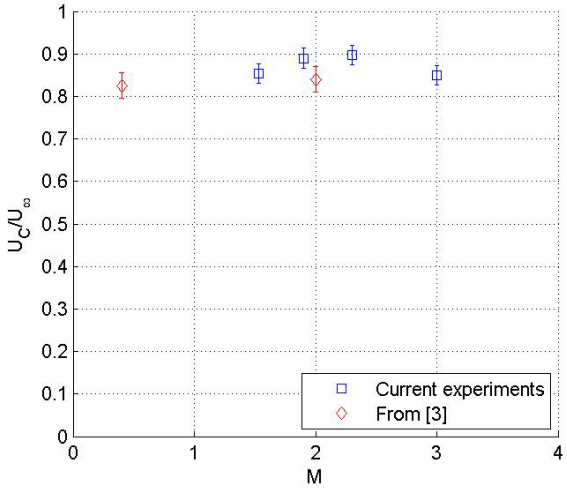

Figure 4. Normalized convective speeds, measured in this work (blue squares) and from [3] (red diamonds).

In order to use this multi-point spectral cross-correlation technique, the convective speed of the traveling mode should be known. As two sub-apertures, adjacent in the streamwise direction, can be treated as a Malley probe, the convective speed can be measured by performing the spectral cross-correlation between two beams, see [17] for details. Figure 4 shows the convective speeds for $M = 1.5$ and 2.3 cases, normalized by the corresponding freestream speed. Normalized convective speeds from [4] are also presented for comparison. The normalized convective speed was observed to moderately increase with the Mach number increasing; this observation is consistent with the model prediction from [4].

Once the convecting speed is known, the stationary and traveling modes can be extracted from the original signal, solving a system of equations (5) for all possible Δx's. A demonstration of this technique is shown in Figure 5, where the original and the extracted stationary and the traveling spectra are calculated for $M = 1.5$. The stationary spectrum, related to mechanical vibrations of the tunnel and the optical components dominates the total spectrum at low frequencies, below 1 kHz. Above 1 kHz, the traveling spectrum, related to the convecting aero-optical boundary layer structures, is the leading source of the total spectrum. The noise-reducing feature of the cross-correlation technique is clearly visible at the high end of the spectrum, above 40 kHz, where the traveling spectrum has a steeper slope, compared to the total spectrum; the slope of traveling spectrum agrees quite well with the theoretically-predicted slope [3], shown in Figure 5 as a dashed line.

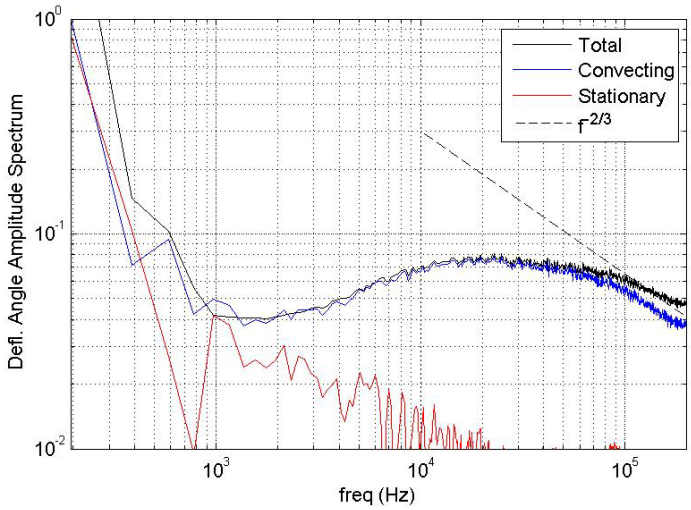

Figure 5. Different components of the deflection angle amplitude spectrum. The theoretically-predicted slope at the high-end of the spectra is also shown is a dashed line. M=1.5, middle of the test section window.

After travelling spectra are extracted, one can investigate the effect of different Mach numbers on the boundary-layer wavefront spectra. The defection-angle spectra from this study are shown in Figure 6; the canonical subsonic BL spectrum from [3] is also plotted for comparison. All spectra are plotted in the normalized form, where the frequency is normalized by the boundary-layer thickness, δ, and the freestream speed, U_∞. All spectra show similar shapes compared to the subsonic canonical boundary layer. All presented spectra have peaks at $St = 0.7$, except for the M=2.3 case, where the peak was found to be 0.9. These peak locations are slightly smaller than for the canonical subsonic boundary layer of 0.9, suggesting that low-frequency, large structures are more energetic in TGF boundary layer. This observation is consistent with the tripped nature of the boundary layer, proposed earlier to explain higher values of the aero-optical BL distortions.

Knowing the deflection angle spectra, several important statistical properties of the boundary layer can be computed: overall levels of OPDrms, the aperture function, $G(Ap,\delta)$, and the cross-correlation function, $R(\Delta x/Ap)$ [3]:

$$OPD_{rms}^2 = 2U_c \int_0^\infty \frac{\left|\hat{\theta}_T(f)\right|^2}{(2\pi f)^2} df \tag{6a}$$

$$G(Ap/\delta) \equiv OPD_{rms}(Ap)/OPD_{rms}, \quad where \quad OPD_{rms}^2(Ap) = 2U_c \int_0^\infty AF(Ap,f) \frac{\left|\hat{\theta}(f)\right|^2}{(2\pi f)^2} df \tag{6b}$$

$$R(\Delta x/Ap;Ap)=\int_0^{\infty}K(fAp/U_{\infty},\Delta x/Ap)\frac{\left|\hat{\theta}(f)\right|^2}{(2\pi f)^2}df \tag{6c}$$

Transfer functions *AF* and *K* are given in [3]. Overall levels of normalized OPDrms, computed using (6a) are presented in Figure 7. These levels are very similar to the normalized levels, presented in Figure 3, right, confirming that for boundary layers it is possible to extract spatial statistics from the temporal information. Careful comparison of levels of OPDrms has revealed that the deflection-angles based levels are consistently lower than levels computed directly from spatially-resolved wavefronts. One reason for this difference is that the additional noise was removed from the deflection angle spectra at high frequencies, as demonstrated in Figure 5, thus lowering overall levels of OPDrms. Another reason is that OPDrms, computed from the deflection-angle spectra, correspond to one-dimensional slices of the 2-D wavefronts and therefore, ignore aero-optical distortions in the cross-stream direction.

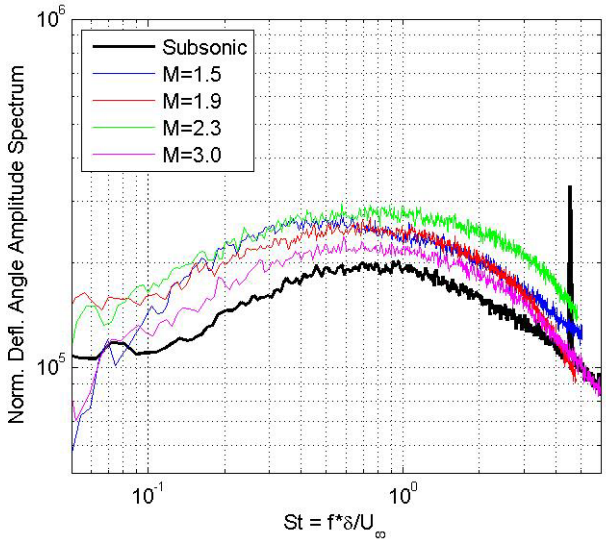

Figure 6. Normalized deflection-angle spectra for different Mach numbers. Re = 3M/ft. The spectrum for subsonic *M* = 0.4 is from [3].

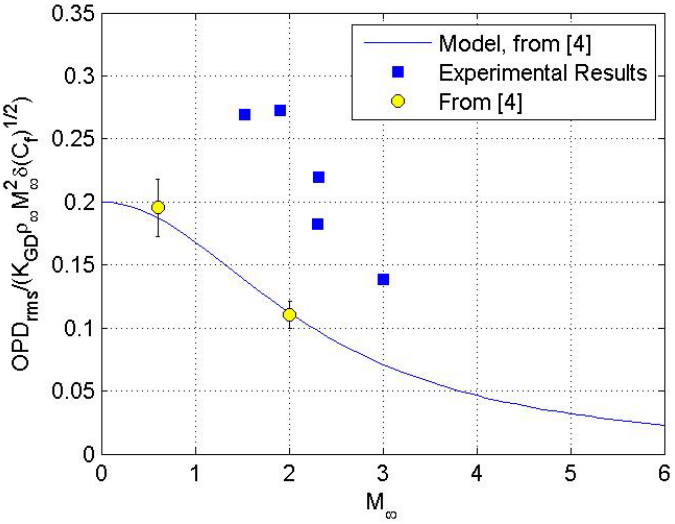

Figure 7. Normalized values of OPD_{rms} calculated from deflection angle spectra, compared with the theoretical prediction [4]. Re = 3 M/ft for M = 1.5, 1.9 and 3.0 and Re = 3M/ft and 4M/ft for M = 2.3.

Aperture functions, $G(Ap,\delta)$, calculated from the traveling component of the deflection angle spectra are presented in Figure 8. The aperture function shows how much optical energy is left in OPDrms after removing aperture-related effects. In [3] it was shown that *AF*-function in (6b) corresponds to a low-pass filter, as effects of

large-scale structure are removed from the aperture-levels of OPDrms. As the large-scale structures were found to be more energetic in TGF, the aperture functions in Figure 8 are consistently lower over a wide range of Ap/δ, compared to the canonical aperture function,

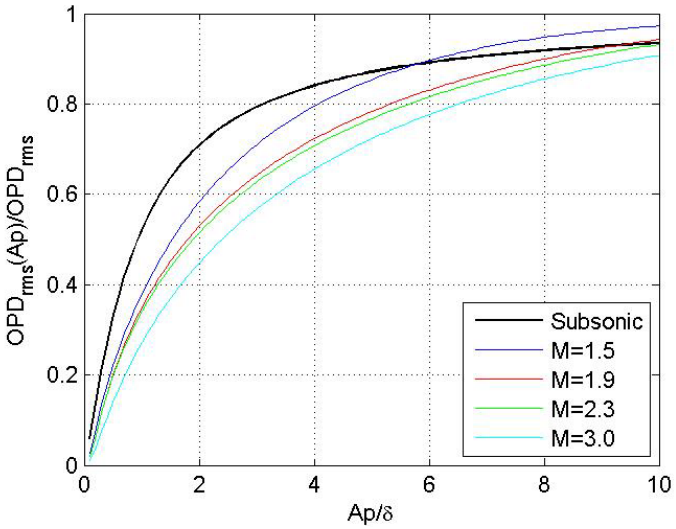

Figure 8. Apetrure Functions, G(Ap/δ), for different Mach numbers. Re =3M/ft.

C. Additional Analysis of Low-Bandwidth WFS Data

Analysis of the Shack-Hartmann wavefront measurements obtained at the lower 25 kHz frame rate reveals that this sampling rate is too small to resolve all of the dynamics of the supersonic TBL in time. This is clearly observed in comparing deflection angle spectra extracted from 25 kHz Shack-Hartmann wavefront measurements and spectra computed from 397 kHz data, shown in Figure 9. Note that there is a poor comparison between the two results. This is due to a significant amount of spectral aliasing that occurs in the 'under-sampled' 25 kHz wavefront data, which results in a substantial buildup of energy at low frequencies ($f \sim 1 - 12$ kHz) such that there is no agreement between the 25 and 397 kHz data in any range of aero-optical interest.

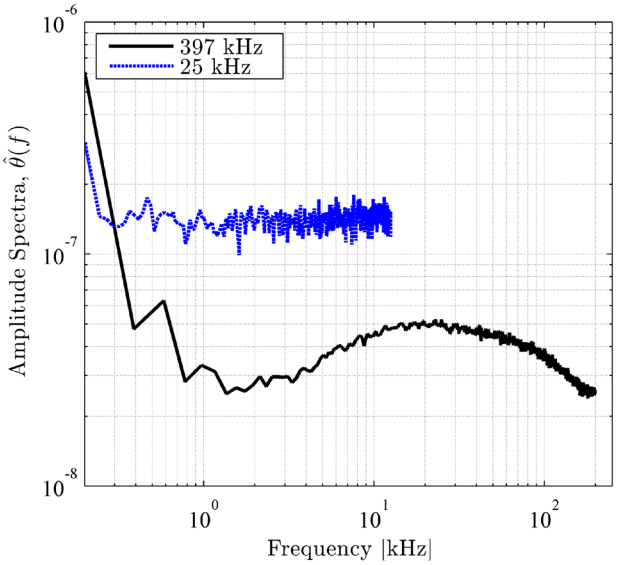

Figure 9. Comparison of supersonic TBL deflection angle spectra calculated from well-sampled and under-sampled data.

Clearly, the temporal resolution of the "undersampled" 25 kHz wavefronts is not sufficient to extract any relevant information about aero-optical properties of the supersonic boundary layers. However, it has a better spatial

resolution, 30×30 subapertures, compared to a limited, 8×3 sub-aperture spatial resolution of the temporally resolved wavefront data. From the high-speed wavefront measurements, see Figure 4, the convection velocity U_C for the $M = 1.5$, was found to be $0.85U_\infty$. A dispersion curve analysis [18] of the 25 kHz wavefront time series, shown in Figure 10, shows a good agreement with this result, although resolution of the branch that corresponds to travelling aero-optic structures is relatively poor.

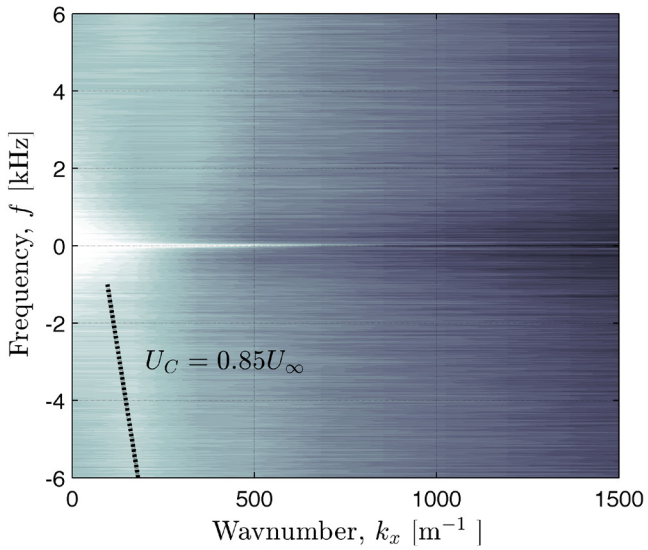

Figure 10. Dispersion curve analysis of 25 kHz wavefront measurements. Convection velocity $U_C = 0.85U_\infty$ is calculated from Malley probe 1-D wavefront measurements.

To overcome these limitations in temporal sampling rate, it has been shown that the frozen-flow assumption from [16] can be used to convert spatially-resolved measurements of wavefront data from individual frames of 2-D wavefront into an estimate of wavefront time series by the relation $t = x/U_C$, where U_C is the convection velocity of aero-optic structures [3]. Spatially resolved measurements of deflection angle from the 25 kHz Shack-Hartmann data can be converted into time series from each frame in a similar manner.

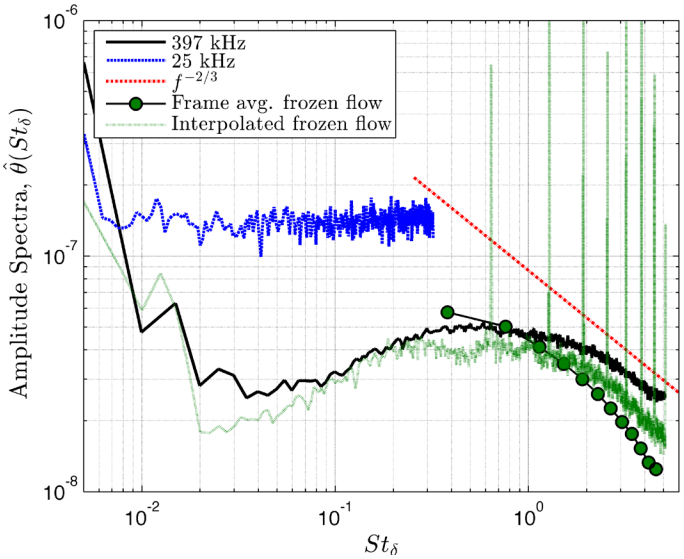

Figure 11. Comparison of wavefront spectra computed by different methods from 'under-sampled' Shack-Hartmann wavefront data.

Using the convection velocity U_C, streamwise strips of wavefront data were extracted from each frame of the 25 kHz data and converted into short time series via the aforementioned method. Then frequency spectra were computed for each one of these short pseudo-time series and the results were averaged across all frames of the 2-D wavefront measurements. These results, presented by filled circles in Figure 11, show good agreement with the deflection angle spectra computed for the 397 kHz data at the high end (f > 15 kHz) of the frequency range. However since the ratio of beam aperture size to the estimated boundary layer thickness, Ap/δ, is approximately 2, spectra from these data are also not able to recover the peak location of the boundary layer aberrations.

To obtain longer time-series of deflection angle data from this frozen-flow approximation method, the pseudo-time series of deflection angles were assigned an 'absolute' time coordinate,

$$t_{absolute} = t_{frame} + \frac{x_j}{U_C} = t_{frame} + t_j,$$

where t_{frame} is the time each consecutive frame was obtained at, and $t_j = x_j/U_C$ is the pseudo-time corresponding to each lenslet sub-aperture in the streamwise direction. Since there is about a 30 % overlap between consecutive frames of 25 kHz data based on the Malley probe measured convection velocity, the resulting time series $\theta_x(t_{absolute})$ does not have any $\Delta t_{absolute}$ larger than $\Delta x/U_C \approx$ (0.001 m)/(390 m/s) = 2.27 μs = 1/(390 kHz), although the time series is not guaranteed to be sampled at uniform intervals. To compute the spectra of these deflection angles, $\theta_x(t_{absolute})$ was interpolated onto a uniform grid corresponding to a 390 kHz sampling rate and then the amplitude spectra was computed. The result of this procedure is shown as a green line in Figure 11. The resulting spectra from the interpolated 25 kHz measured deflection angles shows relatively good agreement between the low-frequency (f < 20 kHz). The general shape of the 397 kHz-sampled data is recovered by this technique, although there are additional sources of numerical interference introduced at regularly spaced intervals above 25 kHz.

For "overlapping" wavefronts it is also possible to estimate the convective speed from "undersampled" data. Recall that wavefronts mostly convect, $W(x, t) = W(x - U_C t)$, or, equivalently for the deflection angles, $\theta(x, t) = \theta(x - U_C t)$, and the temporal evolution of the deflection angle at a point x0 + Δx is approximately the same as at the point x0, but at an earlier time, t - Δt, if $\Delta x = U_C \Delta t$. If the time-shifted cross-correlation is computed,

$$C(\Delta x, \Delta t = 1/f_{samp} = fixed) = \langle \theta(x,t)\theta(x+\Delta x, t+\Delta t) \rangle_{x,t},$$

the location of the peak correlation allows one computing the convective speed. Example of the normalized time-shifted cross correlation for M=1.5 is shown in Figure 12. The location of the peak is at Δx = 0.015 m, which, for the sampling rate of 25 kHz, gives the convective speed of 375 m/sec, or 0.85 of the freestream speed, consistent with results in Figure 4.

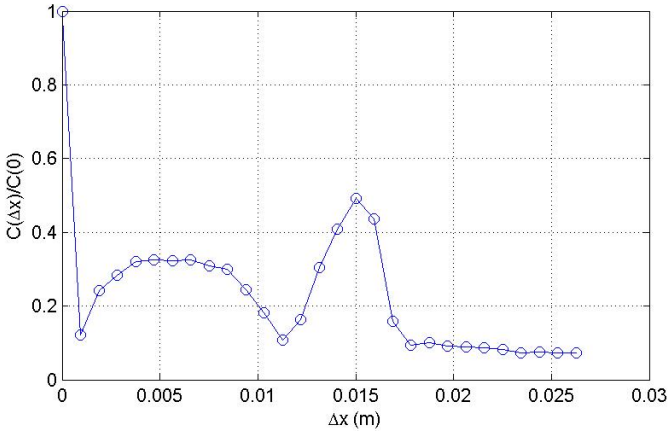

Figure 12. Time-delayed, cross-correlation function C, normalized by C(0), for M = 1.5.

For this method of temporal bandwidth from spatially-resolved 2-D wavefront measurements, there are several key criteria that must be met. First, the frozen-flow assumption must be valid in the aero-optically active flow of interest. There also should not be any significant change in the characteristics of the flow of interest over the aperture, including significant boundary layer growth, shocks, or flow separation. In addition, the original camera frame rate must be high enough that $U_C \Delta t_{samp} < Ap$, which would ensure that the distance each measured wavefront convects is less than one aperture diameter, so apertures can be overlapped. This equation can written as,

$$Ap > \frac{U_C}{f_{samp}},$$

where f_{samp} is the camera frame rate. The minimum diameter, d_{sub} , of each sub-aperture is determined by requiring that pseudo-time step between consecutive sub-apertures, $\Delta t_j = d_{sub}/U_C$, is small such that the corresponding Nyquist frequency is at least ten times larger than the peak frequency expected from the aero-optically active flow. As for the boundary layer with the thickness of δ the peak frequency corresponds to a Strouhal number $St_\delta = f_{peak}\delta/U_\infty = 1$, the time step can be estimated to be

$$\frac{1}{\Delta t_j} = \frac{U_C}{d_{sub}} > 10 \cdot 2 f_{peak} = 20 \frac{U_\infty}{\delta}.$$

It follows that the sub-aperture diameter should be,

$$d_{sub} < 0.05\delta\left(\frac{U_C}{U_\infty}\right).$$

The number of sub-apertures, N_{sub}, required is then simply given as the ratio of Ap/ d_{sub},

$$N_{sub} = \frac{Ap}{d_{sub}} > \frac{U_C}{f_{samp}} \cdot \frac{20}{\delta}\left(\frac{U_\infty}{U_C}\right) = 20 \frac{U_\infty}{\delta \cdot f_{samp}},$$

For the 25 kHz wavefront case which this technique was applied, these equations indicate that the d_{sub} should be approximately less than 0.85 mm; the actual value was 0.94 mm, but the results in Figure 11 indicate that this small difference is acceptable.

IV. Conclusions

Measurements of the aero-optical environment of the compressible boundary layer for a range of supersonic Mach numbers and Reynolds numbers between 1 million per foot and 4 million per foot in TGF facilities in Wright-Patterson Air Force Base are presented. Two data sets were collected with different spatial and temporal resolution using a high-speed Shack-Hartmann wavefront sensor. One data set has detailed, 30x30 subapertures, spatial wavefront information, but with a low, 25 kHz, sampling rate. A second data set has much-higher sampling rate of approximately 400 kHz, but with a limited, 8x3 subapertures, spatial resolution. A multi-point spectral cross-correlation technique was introduced and was shown to be effective in extracting the traveling component of the wavefront spectrum in the presence of a stationary mode and random noise. Overall levels of OPDrms, convective speeds and deflection angle spectra and other useful statistical information were extracted from wavefront data.

It was shown that using the frozen flow assumption, spatially resolved 2-D wavefront measurements that are under-sampled in time can be used to recover temporally resolved measurements of wavefront data, provided that several requirements are met. These requirements include that there be at least some spatial overlap between consecutive frames of wavefront data, and that the lenslet resolution is large enough to capture the dynamics of the aero-optic phenomenon of interest. This technique is only recommended for 'clean' flow, in which no separation occurs and there is a bulk convective velocity, and for measurement applications where there is no significant change in flow characteristics over the entire length of the aperture. This technique was applied to M = 1.5 boundary layer measurements sampled at 25 kHz, and the results compared favorably with measurements of the same flow obtained at a higher sampling rate of 397 kHz.

Analysis of overall levels of aero-optical distortions due to the boundary layer was performed from both data sets and results agree with each other well. The levels of OPDrms were found to be approximately 2-3 larger than for canonical turbulent boundary layers. Deflection angle spectra also revealed that the boundary layer in TGF has slightly more energetic large-scale structures, compared to the canonical boundary layer. All of it suggested that the boundary layer in TGF is most probably tripped somewhere upstream of the test section and the boundary layer in the test section is in almost, but not quite-recovered state. Analysis of the aero-optical properties of the boundary layers tripped by a small back-step [19] has shown that while the wavefront spectrum shape quickly recovers to the canonical shape, the levels of the aero-optical distortions stay elevated for at least 100 back-step heights.

Acknowledgments

This work was supported with in-house and contract funding from the Air Force Research Laboratory. The U.S. Government is authorized to reproduce and distribute reprints for governmental purposes notwithstanding any copyright notation thereon.

The authors would like to thank our collaborators at the Aerospace Systems Directorate of the Air Force Research Laboratory, especially Mr. Don Saunders, 1st Lt. Carl Cunnane and Dr. Ryan Schmit for making these test possible and for their faithful support throughout testing and post-test analysis. We would also like to thank the many AFRL personnel and support contractors who contributed to this study in program management, test planning and execution, and instrumentation development.

References

[1] Jumper, E.J., and Fitzgerald, E.J., 2001, "Recent Advances in Aero-Optics," *Progress in Aerospace Sciences,* 37, 299-339.

[2] Wang, M., Mani, A., and Gordeyev, S., "Physics and Computation of Aero-Optics," *Annual Review of Fluid Mechanics*, Vol. 44, pp. 299-321, 2012.

[3] Gordeyev, S., Smith, A.E., Cress, J.A., and Jumper, E.J. "Experimental studies of aero-optical properties of subsonic turbulent boundary layers," *Journal of Fluid Mechanics*, **740**, pp. 214-253, 2014.

[4] Gordeyev, S., Jumper, E.J., and Hayden, T., "Aero-Optics of Supersonic Boundary Layers," *AIAA Journal*, **50**(*3*), 682-690, 2012.

[5] Gordeyev, S., Cress, J.A. and Jumper, E.J., "Far-Field Laser Intensity Drop-Outs Caused by Turbulent Boundary Layers," *Journal of Directed Energy*, **5**(*1*), pp. 58-75, 2013.

[6] Wyckham, C. and Smits, A. 2009 Aero-Optic Distortion in Transonic and Hypersonic Turbulent Boundary Layers. *AIAA Journal*, **47**(*9*), pp. 2158-2168.

[7] Tromeur, E., Garnier, E., and Sagaut, P., "Large-eddy simulation of aero-optical effects in a spatially developing turbulent boundary layer," *Journal of Turbulence*, **7**, 2006.

[8] Tromeur, E., Sagaut, P., and Garnier, E., "Analysis of the Sutton Model for Aero-Optical Properties of Compressible Boundary Layers, " *J. Fluids Eng*. **128**(2), 239-246, 2005.

[9] White, M. and Visbal, M., "Simulation of Aero-Optical Interactions in Transonic Boundary Layers," *AIAA Paper* 2011-3279.

[10] D. J. Wittich III, M. Paul, H. Ahmed, A. Ahmed, A.E. Smith and S. Gordeyev, "Aero-Optic Characterization of Supersonic Boundary Layers in the Trisonic Gasdynamic Facility," to be presented at 45th AIAA Plasmadynamics and Lasers Conference, Atlanta, GA, 2014.

[12] Wolfe, D.B. (2012) *Boundary Layer Measurements in the Trisonic Gas-dynamics Facility Using Particle Image Velocimetery with CO2 Seeding,* MSAE Thesis, Air Force Institute of Technology.

[13] Clark, G.F. (1982) *Trisonic Gasdynamic Facility User Manual*, Report no. AFWAL-TM-82-176-FIMM. Flight Dynamics Laboratory, Air Force Wright Aeronautical Laboratories, WPAFB, OH.

[14] Wittich, D.J., Gordeyev, S., and Jumper, E.J., "Revised scaling of optical distortions caused by compressible, subsonic turbulent boundary layers," AIAA-2007-4009.

[15] Ryan F. Schmit, private communication, U.S. Air Force Research Laboratory, Wright–Patterson Air Force Base, 2013.

[16] Malley, M.M., Sutton, G.W., and Kincheloe, N., "Beam-jitter measurements of turbulent aero-optical path differences," *Applied Optics*, 31(22):4440–4443, Aug 1992.

[17] S. Gordeyev, T. Hayden and E. Jumper, "Aero-Optical and Flow Measurements Over a Flat-Windowed Turret," *AIAA Journal*, vol. **45**, No. 2, pp. 347-357, 2007.

[18] Smith, A.E., Gordeyev, S., and Jumper, E.J., "Recent measurements of aero-optical effects caused by subsonic boundary layers," *Opt. Eng.* **52**(*7*), 071404, 2013.

[19] A. Smith, S. Gordeyev and E. Jumper, "Aero Optics of Subsonic Boundary Layers over Backward Steps," AIAA Paper 2011-3277, 2011.